6334–6349 *Nucleic Acids Research, 2017, Vol. 45, No. 11* *Published online 27 March 2017*
doi: 10.1093/nar/gkx212

Histone deacetylase class-I inhibition promotes epithelial gene expression in pancreatic cancer cells in a BRD4- and MYC-dependent manner

Vivek Kumar Mishra[1], Florian Wegwitz[1], Robyn Laura Kosinsky[1], Madhobi Sen[1], Roland Baumgartner[2], Tanja Wulff[2], Jens T. Siveke[3,4], Hans-Ulrich Schildhaus[5], Zeynab Najafova[1], Vijayalakshmi Kari[1], Hella Kohlhof[2], Elisabeth Hessmann[6] and Steven A. Johnsen[1,*]

[1]Department of General, Visceral and Pediatric Surgery, Göttingen Center for Molecular Biosciences, University Medical Center Göttingen, Justus-von-Liebig-Weg 11, 37077 Göttingen, Germany, [2]4SC AG, Am Klopferspitz 19a, 82152 Planegg-Martinsried, Germany, [3]German Consortium for Translational Cancer Research (DKTK) and German Cancer Research Center (DKFZ), Heidelberg, Germany, [4]Division of Solid Tumor Translational Oncology, West German Cancer Center, University Hospital Essen, Essen, Germany, [5]Department of Pathology, University Medical Center Göttingen, Robert-Koch-Strasse 40, 37075 Göttingen, Germany and [6]Department of Gastroenterology and Gastrointestinal Oncology, University Medical Center Göttingen, Robert-Koch-Strasse 40, 37075 Göttingen, Germany

Received December 19, 2016; Revised March 14, 2017; Editorial Decision March 19, 2017; Accepted March 20, 2017

ABSTRACT

Pancreatic ductal adenocarcinoma (PDAC) is a highly aggressive cancer with a particularly dismal prognosis. Histone deacetylases (HDAC) are epigenetic modulators whose activity is frequently deregulated in various cancers including PDAC. In particular, class-I HDACs (HDAC 1, 2, 3 and 8) have been shown to play an important role in PDAC. In this study, we investigated the effects of the class I-specific HDAC inhibitor (HDACi) 4SC-202 in multiple PDAC cell lines in promoting tumor cell differentiation. We show that 4SC-202 negatively affects TGFβ signaling and inhibits TGFβ-induced epithelial-to-mesenchymal transition (EMT). Moreover, 4SC-202 markedly induced p21 (*CDKN1A*) expression and significantly attenuated cell proliferation. Mechanistically, genome-wide studies revealed that 4SC-202-induced genes were enriched for Bromodomain-containing Protein-4 (BRD4) and MYC occupancy. BRD4, a well-characterized acetyllysine reader, has been shown to play a major role in regulating transcription of selected subsets of genes. Importantly, BRD4 and MYC are essential for the expression of a subgroup of genes induced by class-I HDACi. Taken together, our study uncovers a previously unknown role of BRD4 and MYC in eliciting the HDACi-mediated induction of a subset of genes and provides molecular insight into the mechanisms of HDACi action in PDAC.

INTRODUCTION

Pancreatic ductal adenocarcinoma (PDAC) is a highly aggressive form of cancer and is the fourth leading cause of cancer-related death in the United States with a 5-year survival rate for advanced PDAC of <5% (1). Due to limited diagnostic options, a lack of reliable biomarkers and minimal symptoms during early stages, most patients are diagnosed at locally advanced or metastatic stages of PDAC. Unfortunately, early dissemination and a high recurrence rate limit the possibility of surgical resection in a majority of the cases. Moreover, current therapeutic options are ineffective, which is largely attributed to the rapid development of drug resistance and metastasis. Therefore, understanding the molecular mechanisms controlling tumor cell dissemination and metastasis may open new avenues for novel drug development and enhanced patient survival.

PDAC is generally associated with key genetic alterations including activating mutations of the *KRAS* oncogene (>95% cases) and inactivating mutations in tumor suppressor genes *TP53, SMAD4* and *CDKN2A* (2,3). However, recent genomic studies have unraveled the complex mutational background of PDAC and the involvement of altered expression of genes controlling key cellular activities including cell cycle regulation, TGFβ signaling, chromatin remodeling and DNA damage repair (4–8). These studies provide a deeper insight into the diverse molecular basis of

*To whom correspondence should be addressed. Tel: +49 551 39 13711; Fax: +49 551 39 13890; Email: steven.johnsen@med.uni-goettingen.de

PDAC and may provide novel treatment options for therapeutic targeting based on the specific molecular defects of individual tumors. Notably, the reversible nature of epigenetic events and associated chromatin modifications provide an exciting opportunity for therapeutic intervention as a monotherapy or in combination with standard therapies.

Chromatin structure is highly dynamic in nature. Post-translational modifications of histone and non-histone proteins can be rapidly and dynamically added or removed in a context-dependent manner. Notably, histone acetylation is usually associated with transcriptional activation and is dependent on the activity of two classes of enzymes, histone acetyltransferases (HAT) and deacetylases (HDAC) which add or remove acetylation marks, respectively, at specific lysine residues and thereby play crucial roles in epigenetic regulation of gene expression (9). Deregulation of the balance between acetylation and deacetylation or aberrant enzymatic activity of HDACs is frequently associated with different types of cancers including PDAC (10,11). For instance, altered activity of HDACs can result in deregulation of important biological processes including cell proliferation, differentiation, apoptosis and migration (10). Thus, HDACs present a promising target for anticancer therapy and currently several small molecule inhibitors targeting HDACs (HDACi) are either approved or in clinical trials for treatment of various cancers including advanced or metastatic PDAC (9,12,13). Interestingly, overexpression of class-I HDACs (including HDAC1, 2, 3 and 8) in PDAC was found to be correlated with poorly differentiated tumors (14,15). HDACi exert their anticancer activity mainly by inducing a G1 cell cycle arrest, apoptosis and differentiation (16–18). Despite the positive results observed in experimental models, to date HDACi have not yielded promising results in clinical trials for most solid tumors including PDAC (9). Therefore, a better understanding of the molecular mechanisms underlying the action of HDACi is required to design better and more efficient therapeutic strategies for the treatment of PDAC.

The Bromodomain-containing Protein 4 (BRD4) belongs to the BET (bromo- and extraterminal) domain family of proteins which are well characterized 'epigenetic readers' that recognize and bind to acetylated lysine residues on histone and non-histone proteins (19). Importantly, the discovery of highly selective small molecule inhibitors of BET family proteins (BETi) (20,21) has revealed a new therapeutic approach to treat cancer which has shown marked efficacy in experimental models of various types of cancer (22–27). In particular, BRD4 plays an important role in maintaining inflammation- and cancer-induced transcriptional programs (21,28). Notably, in addition to its role in controlling oncogene-regulated transcriptional programs, BRD4 also promotes lineage-specific gene transcription (29,30), further underscoring the important context-specific effects of BETi. Paradoxically, while BETi and HDACi appear to function by affecting competing processes (recognition and removal of acetylation on lysine residues, respectively), combined inhibition of BET proteins and HDACs provided a synergistic effect in inhibiting PDAC cell proliferation *in vitro* and tumor growth *in vivo* (31). However, the complex interplay between HDACi activity and BET protein function is largely unknown.

In this study, we performed transcriptome- and genome-wide studies to examine the effectivity of HDACi in modulating cellular plasticity in PDAC utilizing 4SC-202, a novel small molecule inhibitor which specifically targets class-I HDACs, as well as two other well characterized class-I HDACis entinostat and mocetinostat. Notably, 4SC-202 largely inhibited TGFβ-regulated gene expression changes and TGFβ-induced epithelial-to-mesenchymal transition (EMT). Additionally, bioinformatic analysis of the transcriptome- (RNA-Seq) and genome-wide chromatin immunoprecipitation-sequencing (ChIP-Seq) data revealed a potential involvement of BRD4 and MYC in regulating gene expression in response to HDACi. Together, our data demonstrate that inhibiting class-I HDACs promotes a differentiated cell phenotype and that HDACi-mediated induction of a subset of genes involves a cooperative mechanism involving BRD4 and MYC.

MATERIALS AND METHODS

Cell culture

L3.6, BxPC3 and Panc1 cells were purchased from ATCC (Manassas, VA, USA) and cultured in their respective growth media supplemented with 10% fetal bovine serum (Sigma), 1× Pen/Strep (Sigma) at 37°C under 5% CO_2. L3.6 cells were grown in phenol red-free Minimum Essential Medium Eagle (MEM; Invitrogen) containing 1× L-glutamine, BxPC3 cells in phenol red-containing Roswell Park Memorial Institute (RPMI; Invitrogen) 1640 medium and Panc1 cells in phenol red-free Dulbecco's modified Eagle's medium/F-12 (DMEM/F-12; Invitrogen) growth medium. The authenticity of all cell lines used in this study was authenticated by DNA profiling using eight different and highly polymorphic short tandem repeat (STR) loci. Cells were treated with 4SC-202 (1 μM), mocetinostat (500 nM, Selleckchem), entinostat (500 nM, Selleckchem), JQ1 (250 nM) or DMSO (vehicle) for 24 or 72 h and TGFβ (5 ng/ml; R&D systems) for 72 h as indicated. siRNA transfections were performed using Lipofectamine® RNAiMAX (Invitrogen) according to the manufacturer's instructions. SmartPool® siRNA against MYC (Dharmacon) contained the following sequences: 5′-AACGUUAGCUUCACCAACA-3′, 5′-GGAACUAUGACCUCGACUA-3′, 5′-GAACACACAACGUCUUGGA-3′, 5′-CUACCAGGCUGCGCGCAAA-3′. siGENOME non-targeting siRNA (Dharmacon; D-001206-13) was used as a negative control.

Quantitative real-time PCR and western blot

RNA was isolated from 70–80% confluent cells (each well of a 6-well plate) using QIAzol® reagent (Qiagen) according to the manufacturer's instructions. Total RNA (1 μg) was used for performing reverse transcription using the M-MuLV reverse transcriptase (NEB) as described previously (32). Real-time PCR reactions were performed in triplicate using a CFX Connect™ Real-Time System (Bio-Rad) in a total reaction volume of 25 μl. Cycling conditions for real-time PCR were as follows: 95°C for 2 min followed by 40

cycles of 95°C for 15 s and 60°C for 1 min. Cycling conditions for ChIP-qPCR were as follows: 95°C for 2 min followed by 46 cycles of 95°C for 10 s and 60°C for 30 s. The expression levels of target genes were quantitated using SYBR Green I (Invitrogen) and normalized to the reference gene *RPLP0* using a standard curve made from all samples. Relative expression is shown as fold induction relative to the vehicle-treated control sample. ChIP samples were normalized to their corresponding input DNA and shown as percent enrichment relative to input. Error bars represent standard deviations from three independent biological replicates (two technical repeats for each sample). Primers were designed using Primer-Blast software from NCBI (https://www.ncbi.nlm.nih.gov/tools/primer-blast/) and purchased from Sigma-Aldrich, Germany. The primers utilized in this study are listed in Supplementary Table S1.

Whole cell lysates were prepared in RIPA buffer containing protease inhibitors and western blotting was performed as described previously (32). Following sonication, samples were boiled at 95°C for 10 min in SDS-containing loading dye. Subsequently, samples were subjected to polyacrylamide gel electrophoresis (PAGE). Antibodies against specific proteins utilized in this study are listed in Supplementary Table S2.

Migration assay and immunofluorescence staining

Transwell migration assays were performed as described previously (32). Initially, 2.5×10^4 cells were seeded into cell culture inserts containing 8.0 μm pores (BD Biosciences). The following day, cells were treated with either 4SC-202 or vehicle and allowed to migrate for another 48 h. After removing the cells on the inner side of the inserts, migrated cells were fixed with 100% methanol for 10 min and subsequently stained with 0.1% (w/v) crystal violet dissolved in 2% (v/v) ethanol for 10 min.

Immunofluorescence staining was performed as described previously (33). Briefly, cells grown on coverslips were fixed with 4% paraformaldehyde for 10 min and permeabilized with 0.1% Triton X-100 in PBS. Blocking was performed with 10% FBS in PBS and subsequently the coverslips were incubated with the primary antibody diluted in blocking solution overnight at 4°C. The following day, cells were incubated with conjugated secondary antibodies at room temperature and subsequently nuclei were stained with DAPI (Sigma, D9542). The coverslips were mounted on glass slides using mounting medium (Dako, S3023). Fluorescent staining was observed using an AXIO Scope.A1 microscope (Zeiss) and images were processed with the ZEN 2 lite software. Primary and secondary antibodies utilized in this study are listed in Supplementary Table S2.

Cell proliferation assay and quantification

To measure the proliferation capacity of the cells, 10 000 cells were seeded in each well of a 6-well plate. Cells were treated with 1 μM 4SC-202 for 7 days, fixed with 100% methanol for 10 min and cells were stained with 0.1% crystal violet solution for 20 min at room temperature. Plates were scanned and quantification was performed by using ImageJ software (34). The average of three biological replicates was used to perform the analysis and data are shown as 'relative % area'.

Sphere formation assay

The sphere formation assay was performed in Corning® 96-well clear flat bottom ultra-low-attachment microplates. Cells were trypsinized and 500 cells/well were seeded in serum-free DMEM/F12 medium containing 5 ng/ml insulin, 20 ng/ml basic fibroblast growth factor (bFGF), 2% B27 (serum-free supplement), 20 ng/ml epidermal growth factor (EGF) and 1% N2-supplement (35). The following day the cells were treated with DMSO or 4SC-202 and grown for 7 days. The number of spheres in each well was counted microscopically and the average of biological triplicates was used for quantitation and statistics.

Xenograft study

For each animal, one million tumor cells were resuspended in 20 μl of a 1:1 mixture of DMEM medium and BD Matrigel Matrix High Concentration (HC), Growth Factor Reduced (GFR) (BD Bioscience) and kept on ice until transplantation. Nine week old virgin NMRI foxn1nu/nu mice (Janvier Labs) were anesthetized by isoflurane inhalation (2–3%, Forene). The cell suspensions were injected under sterile conditions subcutaneously with a 0.3 ml Micro-Fine syringe (BD Bioscience) into the left abdominal flank. After tumors were palpable (size = 100 mm^3), mice were randomly divided into two groups ($n = 12$ per group) as control and treated. Animals were treated with either vehicle (methylcellulose) or 4SC-202 (120 mg/kg in methylcellulose) for 4 days (b.i.d) via oral gavage and then followed for another week until sacrificing. Mouse weight and tumor size were measured daily.

Chromatin immunoprecipitation, library preparation and next-generation sequencing

Chromatin immunoprecipitation (ChIP) was performed in L3.6 cells treated with DMSO or 4SC-202 in three biological replicates for each condition as described previously (30). Briefly, cells were cross-linked with 1% formaldehyde (in PBS) for 20 min (for BRD4) or 10 min (for histone modifications) at room temperature. Cross-linking was quenched by adding 1.25 M Glycine for 5 min. Cells were lysed, collected by scraping and nuclear pellets were washed in a nuclear preparation buffer consisting of 5 mM EDTA, 150 mM NaCl, 50 mM Tris–HCl (pH 7.5), NP-40 (0.5%, v/v), Triton X-100 (1%, v/v). Nuclear pellets were resuspended in the lysis buffer and sonicated using a Bioruptor® Pico (Diagenode) with 30 s on/off pulse. After sonication, precleared (50% Sepharose 4B from GE Healthcare) chromatin extract was subjected to immunoprecipitation by overnight incubation with the specific antibody. Non-specific IgG was used as a negative control. The following day, samples were incubated with Protein-A Sepharose (GE Healthcare) for 2 h at 4°C, immune complexes were washed, de-crosslinked and DNA was extracted.

Prior to library preparation, DNA samples were sonicated again for 40 cycles (total volume 10 μl) to ensure

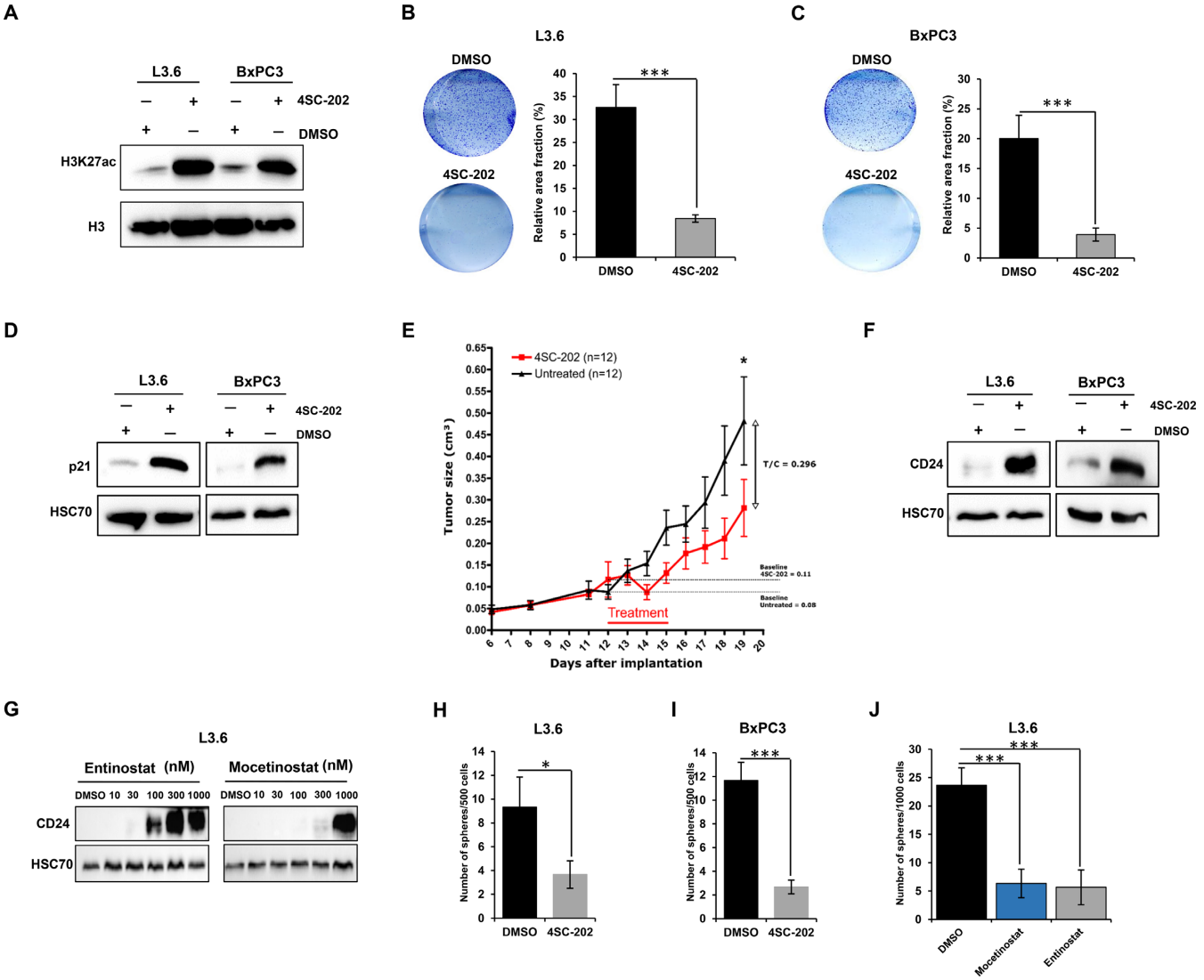

Figure 1. 4SC-202 exerts growth inhibitory and differentiation-promoting effects. (**A**) Western blot analysis of H3K27ac in L3.6 and BxPC3 cells treated either with 1 μM 4SC-202 or DMSO (control cells). Total H3 was used as a loading control. (**B**, **C**) Cell proliferation assays were performed in L3.6 and BxPC3 cells to determine the anti-proliferative effects of 4SC-202. Cells were treated either with 4SC-202 or DMSO (control) and allowed to grow for 5 days. Colonies formed were visualized by staining with 0.1% crystal violet solution. Stained areas (left) were quantified and displayed as 'relative fraction area' (right). Data are represented as mean ± SD. $n = 3$. $^{***}P \leq 0.005$, $^{**}P \leq 0.01$, $^{*}P \leq 0.05$. (**D**) Western blot analysis of p21 protein levels in L3.6 and BxPC3 cells following 4SC-202 treatment. HSC70 was used a loading control. (**E**) Anti-tumor effects of 4SC-202 were examined by xenograft studies. Cells were implanted into immune-deficient mice and allowed to develop into tumors. Mice were randomly divided into two groups ($n = 12$) and treated either with vehicle or 4SC-202 for 4 days (twice daily). The graph depicts the tumor volume recorded daily for 12 days and T/C (treatment-to-control ratio) value. (**F**) Western blot analysis of CD24 protein levels in L3.6 and BxPC3 cells following 4SC-202 treatment. HSC70 was used a loading control. (**G**) Western blot analysis of CD24 protein levels in L3.6 cells following mocetinostat or entinostat treatment. (**H**, **I**) Sphere formation assay was performed in L3.6 and BxPC3 cells. Approximately 500 cells were seeded in each well of a 96-well plate and cells were treated with DMSO or 1 μM 4SC-202. The number of spheres was counted microscopically across three wells. Data are represented as mean ± SD. $n = 3$. $^{***}P \leq 0.005$, $^{**}P \leq 0.01$, $^{*}P \leq 0.05$. (**J**) Sphere formation assay was performed in L3.6 cells as described in (H, I). Cells were treated with 500 nM mocetinostat or entinostat.

fragment sizes of ≤300 bp. DNA was quantitated using the Qubit® dsDNA HS assay and a Qubit® 2.0 Fluorimeter (Invitrogen). Three to five nanogram of fragmented DNA was used for generating the ChIP-Seq libraries using the MicroPlex Library Preparation Kit (Diagenode) according to the manufacturer's instructions. Five hundred ng total RNA from L3.6, BxPC3 and Panc1 cells was used to generate RNA-Seq libraries (three biological replicates for each condition) using the NEXTflex Rapid Directional RNA-Seq Kit (Bioo Scientific) following the manufacturer's instructions. Following library preparation, size and quality was checked using a Bioanalyzer 2100 (High Sensitivity DNA assay). Single-end sequencing (50 bp) was performed using the HiSeq 2000 Illumina platform at the Transcriptome and Genome Analysis Laboratory of the University Medical Center Göttingen, Germany.

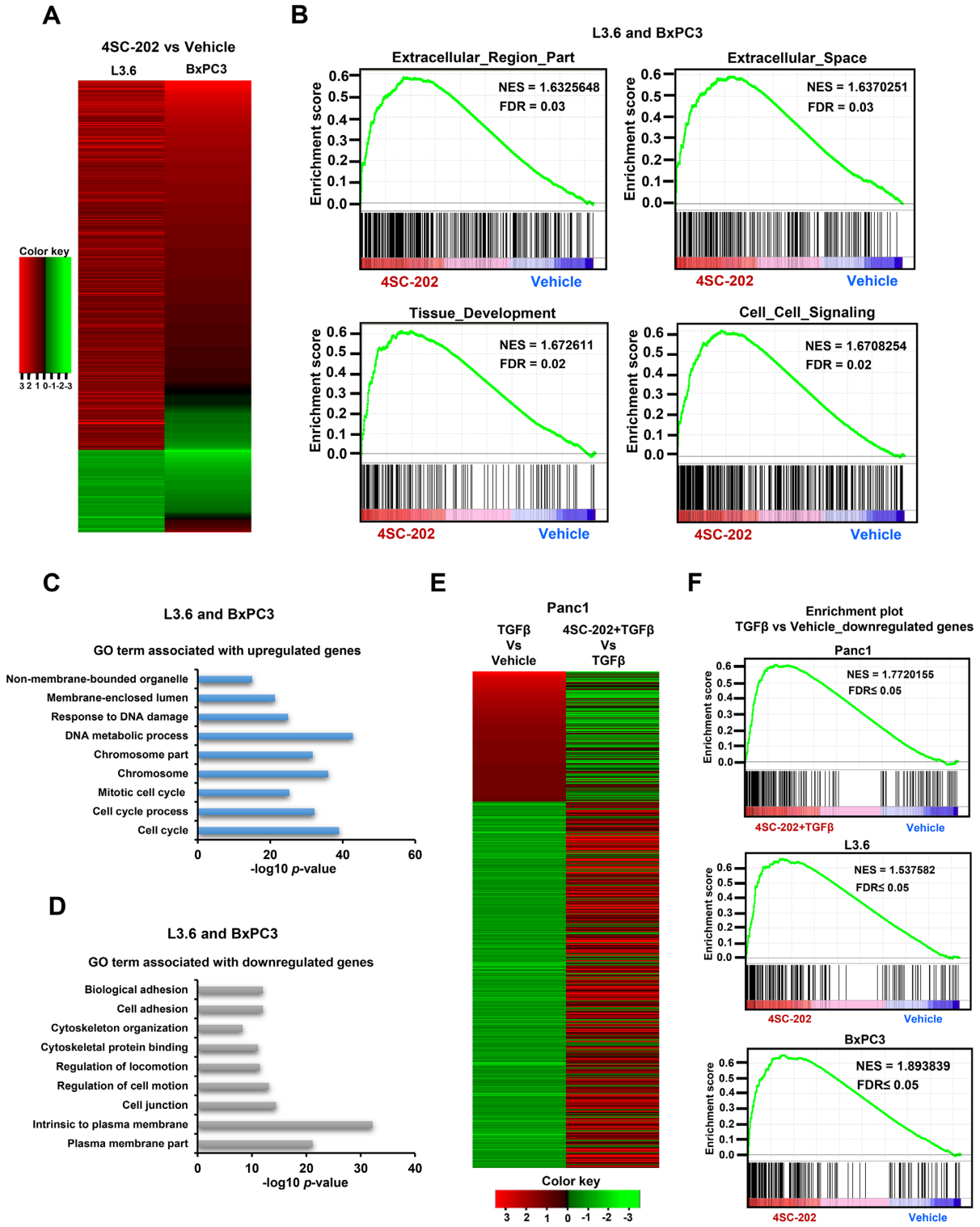

Figure 2. 4SC-202 impairs TGFβ-induced gene expression changes. (**A**) The heatmap depicts the similarity in transcriptome-wide effects of 4SC-202 in L3.6 and BxPC3 cells. Heatmaps were generated by selecting significantly (padj≤0.05) up- ($\log_2$ FC ≥ 0.75, red) or downregulated ($\log_2$ FC ≤ –0.75, green) genes in 4SC-202-treated samples compared to the vehicle-treated samples in either cell line. (**B**) GSEA plots from differentially regulated genes in RNA-Seq data from L3.6 and BxPC3 cells. Significantly enriched pathways are shown. FDR ≤ 0.05 was considered to be significant. In the graph, NES (normalized enrichment score) and FDR (false discovery rate) are indicated. (**C**, **D**) Gene ontology (GO) analysis on biological process (BP) for significantly up- or downregulated genes from L3.6 and BxPC3 cells. Analysis was performed using the DAVID online tool. Plots are shown for significantly enriched pathways. $P_{val} \leq 0.05$ was considered as significant. (**E**) Heatmap depicting the effects of 4SC-202 on TGFβ-regulated genes from RNA-Seq data in Panc1 cells. All genes found to be significantly ($P_{adj} \leq 0.05$) up- ($\log_2$ FC ≥ 1, red) or downregulated ($\log_2$ FC ≤ –1, green) by TGFβ are shown. (**F**) GSEA plots depict the 4SC-202 effects in the three cell lines (Panc1, L3.6 and BxPC3) on a set of genes identified as being downregulated by TGFβ in Panc1 RNA-Seq data. FDR ≤ 0.05 was considered to be significant.

Bioinformatic analysis of ChIP- and RNA-sequencing

Prior to further analysis, a quality control check of the raw sequencing data (FASTQ files) was performed by using FastQC on Galaxy (Galaxy Version 0.65) (36). FASTQ files were aligned to the human reference genome (assembly hg19) using Bowtie2 with very-sensitive pre-sets in end-to-end mode (37). Subsequently, mapped files were utilized to perform peak calling with Model-based Analysis of ChIP-Seq 2 (MACS2) (Galaxy Version 2.1.0.20151222.0) with default settings and *–broad* options (38). The minimum FDR cutoff for peak detection (q-value) was set to 0.05. Normalization (reads per kilobase per million or RPKM) of the ChIP-Seq data was performed using the bamcoverage tool on deepTools (Galaxy Version 2.3.6.0) by utilizing the merged BAM files (39). The normalized ChIP-Seq data was visualized on Integrative Genomics Viewer (IGV) (40). Heatmaps were generated on deeptools2 and aggregate plots on Cistrome Galaxy. Differential binding analysis was performed to determine the H3K27ac-enriched regions using the DiffBind R-package (R version 3.2.2) (41). Genomic Regions Enrichment of Annotations Tool (GREAT) was utilized to determine the genes associated with H3K27ac-enriched regions obtained from DiffBind analysis (42). ReMap (Regulatory Map of Transcription Factor Binding Sites) was used to determine the enrichment of transcription factors and cofactors associated with H3K27ac-enriched regions that were increased, decreased or unchanged upon 4SC-202 treatment (43). BED files for BRD4 and MYC binding sites were downloaded from ReMap.

For RNA-Seq data, FASTQ files were mapped to the reference human transcriptome (hg19) using the TopHat tool on Galaxy with 'very sensitive' and 'end-to-end' Bowtie2 settings. BAM files were sorted using SortSam (version 1.126.0) from Picard tools on Galaxy. The read counting was performed using the HT-Seq tool (version 0.6.0) (with parameters -f bam -r pos -s reverse -a 10 -t exon -m union) (44) and count files were used for differential gene expression analysis using the DESeq2 (45) package on R (Bioconductor version 3.2.2). Heatmaps were generated using heatmap.2 (gplots R package). Gene Set Enrichment Analysis (GSEA) was performed with default settings (1000 permutations for gene sets, Signal2Noise metric for ranking genes). For enrichment of TGFβ-mediated downregulated genes (log2FC≤-1 and $P \leq 0.05$) in L3.6 and BxPC3 cells (4SC-202 vs Vehicle) or Panc1 cells (4SC-202+TGFβ vs TGFβ), predefined gene list based on RNA-Seq data were selected. In other cases, the gene ontology (GO) set c5.all was used for enrichment analysis. GO analysis was performed using the Database for Annotation, Visualization and Integrated Discovery (DAVID) and GO categories with FDR <0.05 considered significant.

Statistical analysis

All data are represented as mean ± SD. For calculating the statistical significance of qRT-PCR data, cell proliferation and sphere formation assay a one-way ANOVA test was used. Two-way ANOVA tests were performed for calculating statistical significance of mouse data. A *P-value* of ≤0.05 was considered as significant. *P-values* ≤0.05, ≤0.01, ≤0.001 are shown as single (*), double (**) and triple (***) asterisks, respectively.

RESULTS

4SC-202 inhibits cell proliferation *in vitro* and *in vivo*

4SC-202 is a novel HDACi, reported to also target Lysine-Specific Demethylase-1 (LSD1) (46), but displaying a high specificity towards class-I HDACs. We sought to specifically examine the potential anti-tumor effects of the HDACi activity of 4SC-202 in PDAC. Initially, we verified the HDACi activity of 4SC-202 by examining global levels of H3K27ac following treatment and observed increased acetylation in two different pancreatic cancer cell lines, L3.6 and BxPC3 (Figure 1A). Consistent with previous studies demonstrating that HDACi modulate cell proliferation, at least in part, by inducing the expression of the cell cycle inhibitor p21 (*CDKN1A*) (47), 4SC-202 significantly decreased proliferation of both cell lines (Figure 1B, C) and concomitantly increased p21 protein levels (Figure 1D). To examine the *in vivo* effects of 4SC-202 treatment, we implanted L3.6 cells into immune-deficient mice and allowed tumors to develop. Subsequently, mice were randomly divided into two groups (n = 12) and treated acutely with either methylcellulose (vehicle) or 4SC-202 for 4 days (b.i.d.) and monitored tumor growth for an additional week. Consistent with the observed *in vitro* effects, tumor size was significantly reduced in 4SC-202-treated mice compared to the vehicle-treated group (Figure 1E). Body weight was routinely monitored in this study and exposure was verified in a separate pharmacokinetics study for 4SC-202 in a cohort of healthy animals using the same treatment dose (Supplementary Figure S1A and B).

A characteristic feature of HDACi in many tumor and cell types is the induction of a more differentiated phenotype (48,49). Since a recent study demonstrated that membranous CD24 expression was correlated with a more differentiated phenotype in PDAC (50), we examined the effects of 4SC-202 treatment on CD24 expression. Notably, CD24 protein levels were significantly increased following 4SC-202 treatment (Figure 1F). Furthermore, we also examined the effects of two other well characterized class-I HDACi entinostat and mocetinostat on CD24 expression. Both inhibitors significantly increased CD24 protein levels (Figure 1G). Given the established connection between high CD24 expression and a differentiated phenotype in PDAC, we next tested the effects of 4SC-202 on stem-cell like characteristics in the cells. The sphere formation assay is a widely used method to assess the clonogenic growth potential of cells, a feature associated with stem cell-like characteristics (51). We observed a significant reduction in sphere-forming abilities of both L3.6 and BxPC3 cells upon 4SC-202 treatment (Figure 1H and I). These findings were confirmed by treating L3.6 cells with mocetinostat and entinostat, which both elicited a similar significant decrease in sphere formation (Figure 1J). Together, these results revealed growth inhibitory and differentiation-promoting effects of 4SC-202 in PDAC cells.

TGFβ-induced gene repression is blocked by 4SC-202

To investigate the transcriptome-wide effects of 4SC-202 on gene expression we performed RNA-Seq studies in L3.6 and BxPC3 cells. Both cell lines exhibited similar responses as depicted in the heatmap displaying all significantly regulated genes ($\log_2$ FC $\pm$ 0.75, $p_{adj} \leq 0.05$) in either cell line (Figure 2A). To obtain a deeper insight into the gene expression patterns altered in response to 4SC-202 treatment we performed gene set enrichment analysis (GSEA). Interestingly, significantly enriched pathways were associated with differentiation-related phenotypes such as tissue development and cell-cell signaling (Figure 2B). Gene ontology (GO) analysis revealed that the genes upregulated in both cells lines upon 4SC-202 treatment were mainly associated with cell cycle-related processes (Figure 2C) while downregulated genes were enriched in pathways involving migration and cell-adhesion (Figure 2D), pointing towards a potential role of 4SC-202 in regulating EMT. To further investigate this possibility, we utilized Panc1 cells, which undergo EMT upon TGFβ stimulation (33,52), and examined the transcriptome-wide effects in combination with TGFβ treatment. As shown in the heatmap in Figure 2E, 4SC-202 significantly attenuated TGFβ-induced gene repression. Based on this observation, we hypothesized that TGFβ-induced gene repression relies upon HDACs and blocking their activity with 4SC-202 could revert this phenotype even in other cell systems. Therefore, we examined the effects of 4SC-202 on the set of TGFβ-downregulated genes ($P_{adj} \leq 0.05$, $\log_2$ FC ≤ -1) identified from Panc1 RNA-Seq data and observed a positive enrichment of this set of genes following 4SC-202 treatment, not only in Panc1 cells, but also both in L3.6 and BxPC3 cells (Figure 2F).

4SC-202 attenuates TGFβ-induced EMT

To confirm the ability of 4SC-202 to block EMT we examined the effect of 4SC-202 on classical epithelial and mesenchymal markers in Panc1 cells following TGFβ stimulation. Consistent with the transcriptome-wide blockade of TGFβ-induced gene expression changes, 4SC-202 significantly attenuated the TGFβ-induced downregulation of mRNA levels of epithelial-related genes (E-cadherin encoded by *CDH1*, *TJP3* and *MMP2*) as well as the upregulation of mesenchymal-related genes (N-cadherin encoded by *CDH2*, *SNAI1* and *ZEB1*; Figure 3A). Consistently, we also observed a similar increase in the protein levels of E-cadherin as well as decreases in the protein levels of the mesenchymal markers ZEB1, Vimentin, N-cadherin and SNAI1 (Figure 3B). These effects were further confirmed in immunofluorescence analyses, where TGFβ-induced downregulation of E-cadherin and upregulation of ZEB1 were blocked by 4SC-202 (Figure 3C). Interestingly, 4SC-202-treatment in Panc1 cells also blocked the TGFβ-induced phosphorylation of SMAD2/3 (Figure 3B), suggesting that it may generally inhibit TGFβ signaling. Notably, downregulation of both ZEB1 and SNAI1 was also observed in both L3.6 and BxPC3 cells as well (Figure 3D), showing that these effects can be observed even in the absence of extrinsic activation of TGFβ signaling. Consistent with the proposed importance of EMT in promoting tumor cell migration and metastasis, it was previously shown that TGFβ treatment enhanced the migratory potential of Panc1 cells (52). Notably, 4SC-202 treatment also attenuated the TGFβ-induced migration of these cells (Figure 3E). Moreover, as observed in the L3.6 and BxPC3 cell lines (Figure 1F), the expression of the epithelial differentiation marker CD24 was increased both at the mRNA (Figure 3F) and protein (Figure 3G) levels following 4SC-202 treatment of Panc1 cells, independent of TGFβ treatment. Similarly, Panc1 cell proliferation was markedly reduced following 4SC-202 treatment (Figure 3H), accompanied by increased p21 protein levels (Figure 3I). Together, these results demonstrate that treatment with 4SC-202 can reverse EMT-associated gene repression.

4SC-202 upregulated genes are co-occupied by BRD4 and MYC

In order to uncover epigenetic regulatory mechanisms underlying the differential effects of 4SC-202 on the regulation of gene expression we performed genome-wide occupancy studies for H3K27ac and H3K4me3, histone marks associated with active transcription, in L3.6 cells. Consistent with the inhibitory function of HDACs in transcriptional regulation, 4SC-202 treatment significantly increased the levels of H3K27ac around the transcriptional start site (TSS) of genes globally (Figure 4A and B). Furthermore, H3K4me3 levels were also increased globally around the TSS of genes upon 4SC-202 treatment (Supplementary Figure S2A, B). Interestingly, genomic regions associated with significant increases in H3K27ac upon 4SC-202 treatment were mainly confined to the 5 kb region around the TSS (Figure 4C). Given the positive correlation between the activating histone modifications and gene expression, we sought to determine whether the 4SC-202-mediated increase in H3K27ac and H3K4me3 marks was associated with changes in gene expression. Thus, we utilized our RNA-Seq data from L3.6 cells to group genes into three categories based on the effects of 4SC-202 treatment on mRNA levels as follows: upregulated ($P_{adj} \leq 0.05$ and $\log_2$ FC ≥ 1), unchanged ($P_{adj} > 0.8$, abs($\log_2$ FC) $\leq \pm 0.2$) and downregulated ($p_{adj} \leq 0.05$, $\log_2$ FC ≤ -0.75) upon 4SC-202 treatment. Surprisingly, H3K27ac and H3K4me3 levels were consistently increased around the TSS of all the three groups of genes to a similar extent in response to 4SC-202 treatment, irrespective of the effects on gene expression (Supplementary Figure S2C and D). Given the similarity in the effects of HDACi treatment on the occupancy of activating histone marks around the TSS of genes, we hypothesized that different transcription factors (TFs) and co-factors may be required for the differential effects of 4SC-202 treatment on target gene expression. Therefore, we utilized the ReMap (Regulatory Map of TF Binding Sites) analysis tool (43) to identify potential factors whose occupancy overlapped that of proximal H3K27ac-enriched regions associated with upregulated, unchanged and downregulated genes. As expected, all three categories were enriched for general TFs such as TBP and TAF1. However, only the TSS of upregulated genes showed an enrichment of BRD4 and MYC among the top ten most highly enriched factors (Figure 4D and Supplementary Figure S2E, F). Notably, 551 out of 618 H3K27ac-enriched regions associated with upregu-

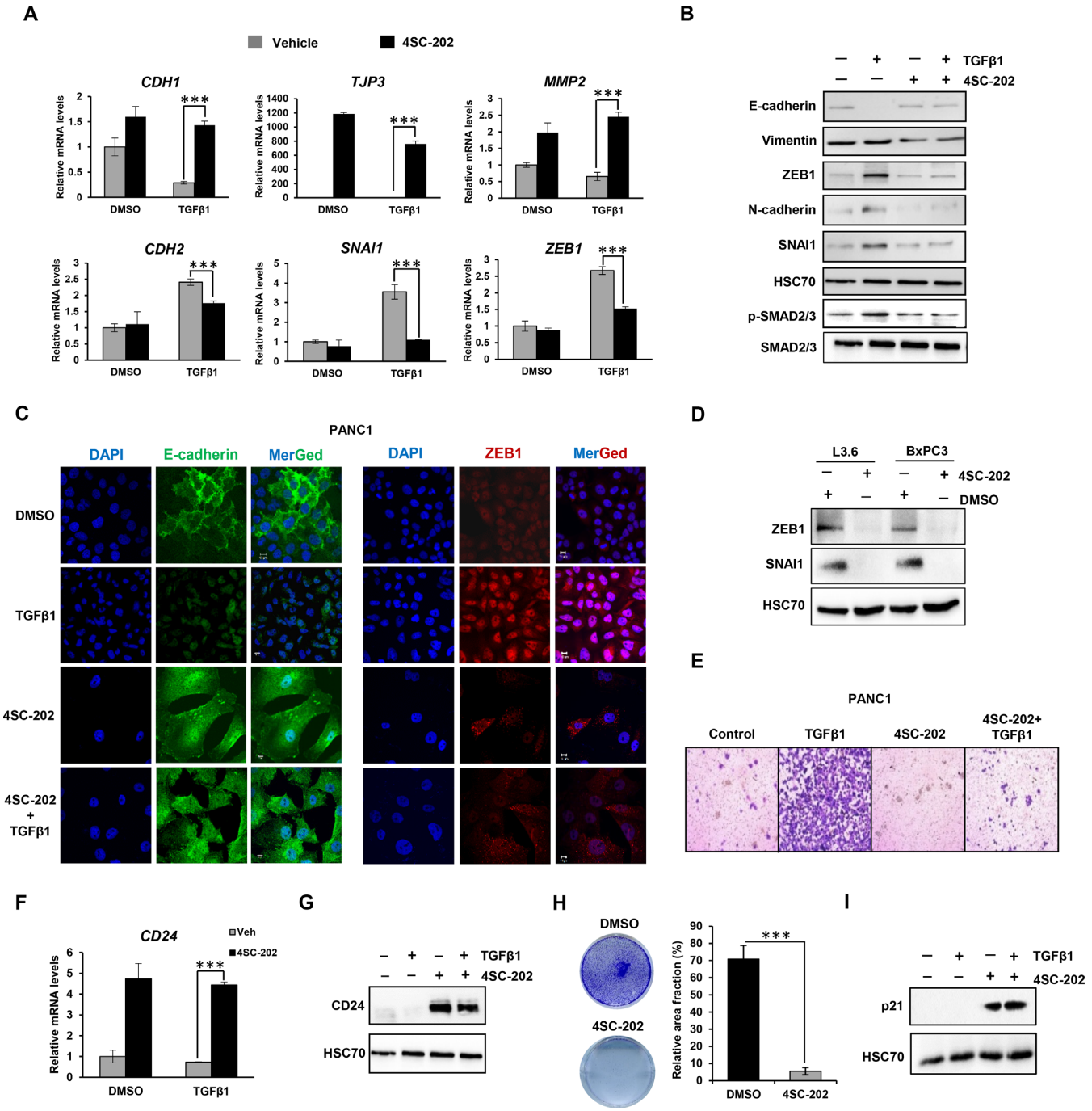

Figure 3. 4SC-202 attenuates TGFβ-induced EMT. (**A**) Gene expression analysis of epithelial (upper panels) and mesenchymal markers (lower panels) in Panc1 cells. Cells were treated with 5 ng/ml TGFβ and/or 4SC-202 (1 μM) and DMSO (vehicle) for 72 h. The relative expression of epithelial markers (*CDH1*, *TJP3* and *MMP2*) and mesenchymal markers (*CDH2*, *SNAI1* and *ZEB1*) were analyzed by qRT-PCR and are shown as 'relative mRNA levels' compared to the expression of an unregulated reference gene (*RPLP0*). Data are represented as mean ± SD. $n = 3$. ***$P \leq 0.005$, **$P \leq 0.01$, *$P \leq 0.05$. (**B**) Western blot analysis of epithelial (E-cadherin) and mesenchymal markers (N-cadherin, Vimentin, SNAI1, ZEB1) and phosphorylated SMAD2/3 in Panc1 cells. Cells were treated as in (A). HSC70 was used as a loading control. (**C**) Immunofluorescence staining for epithelial (E-cadherin) and mesenchymal (ZEB1) markers in Panc1 cells treated as in (A). Nuclei were stained with DAPI. Scale bar represents 10 μm. (**D**) Western blot analysis of ZEB1 and SNAI1 in L3.6 and BxPC3 cells following 4SC-202 treatment. HSC70 was used as a loading control. (**E**) Transwell migration assay was performed in Panc1 cells treated as in (A). Migrated cells were stained with 0.1% crystal violet and visualized microscopically. (**F**) Gene expression analysis of *CD24* in Panc1 cells. Relative expression of *CD24* was analyzed by qRT-PCR and is shown as 'relative mRNA levels' compared to the expression of an unregulated reference gene (*RPLP0*). Data are represented as mean ± SD. $n = 3$. ***$P \leq 0.005$, **$P \leq 0.01$, *$P \leq 0.05$. (**G**) Western blot analysis of CD24 in Panc1 cells as in (B). HSC70 was used as a loading control. (H) Cell proliferation was analyzed in Panc1 cells treated with 4SC-202 or DMSO. Stained areas (left) were quantified and displayed as 'relative area fraction' (right). Data are represented as mean ± SD. $n = 3$. ***$P \leq 0.005$, **$P \leq 0.01$, *$P \leq 0.05$. (**I**) Western blot analysis of p21 protein levels in Panc1 cells treated with TGFβ and/or 4SC-202 and control cells treated with DMSO as in (B and G). HSC70 was used as loading control.

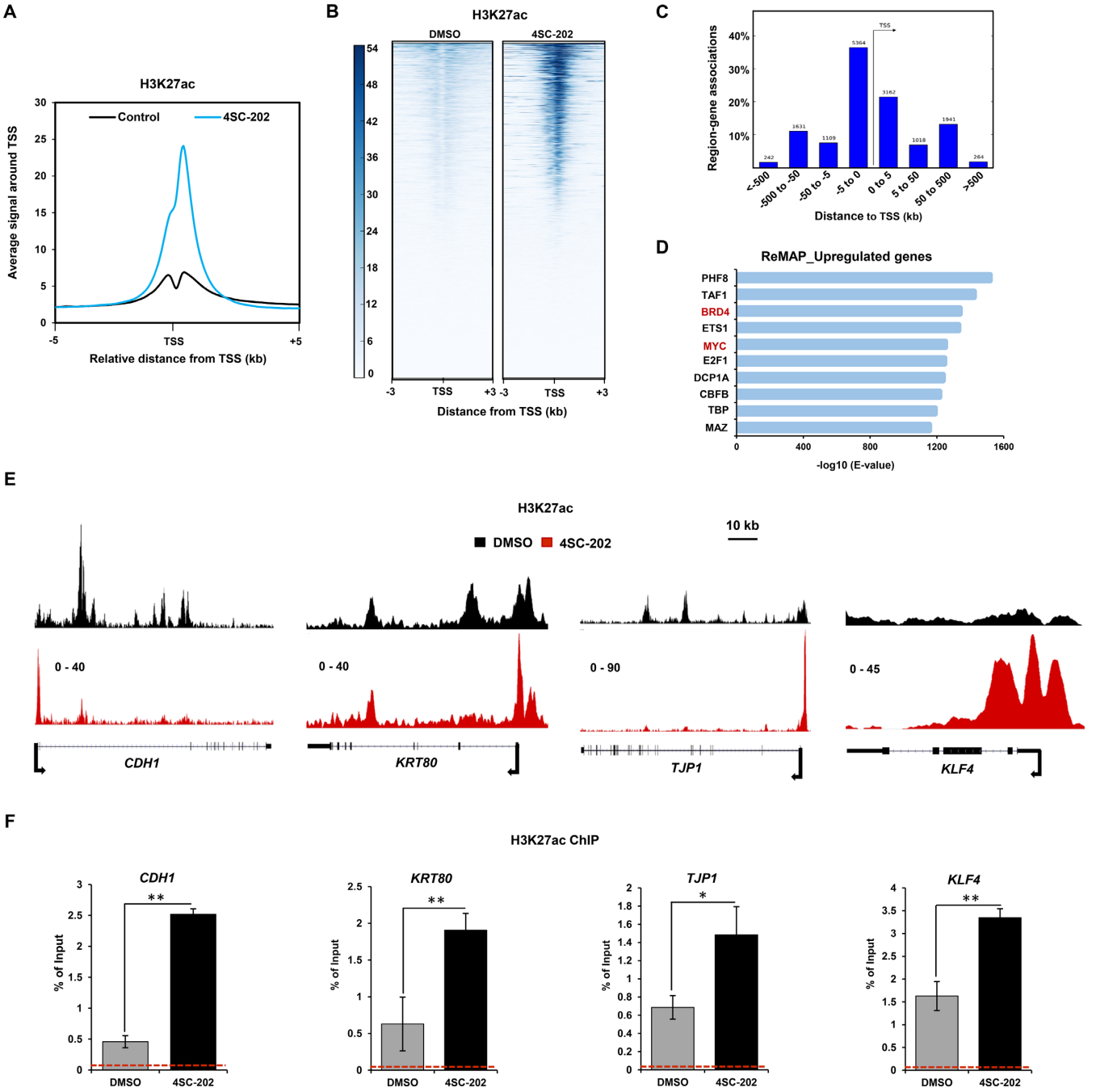

Figure 4. Genes upregulated by 4SC-202 and displaying increased H3K27ac levels are enriched for BRD4 and MYC occupancy. (**A**) Average intensity profile of normalized H3K27ac (RPKM) signals around the TSS (±5 kb) of the genes in L3.6 cells treated with DMSO or 4SC-202. (**B**) Heatmaps depict the average occupancy of H3K27ac around the TSS (±3 kb) of all genes in L3.6 cells treated with DMSO or 4SC-202. (**C**) GREAT analysis was performed on regions displaying increased H3K27ac following 4SC-202 treatment obtained from DiffBind analysis. Bar graph from GREAT analysis shows the enrichment and orientation of H3K27ac-enriched regions relative to the nearest TSS. (**D**) ReMAP analysis was performed on H3K27ac-enriched regions associated with upregulated ($P_{adj} \leq 0.05$ and $\log_2$ FC ≥ 1) genes upon 4SC-202 treatment. Top 10 significantly enriched hits ($\log_{10}$-E-value) are shown in the bar graph. (**E**) H3K27ac profile for a subset of 4SC-202-upregulated genes (*CDH1*, *KRT80*, *TJP1* and *KLF4*) in L3.6 cells in control (DMSO, black) and 4SC-202-treated (red) conditions. Scale bar represents 10 kb. The black arrow indicates the TSS and direction of transcription. (**F**) ChIP analysis of H3K27ac on the TSS of the *CDH1*, *KRT80*, *TJP1* and *KLF4* genes in L3.6 cells treated with 4SC-202. Immunoprecipitated DNA was compared to input and shown as percentage. IgG was used as a negative control to indicate experimental background and is shown as a red dotted line. Data are represented as mean ± SD. $n = 3$.

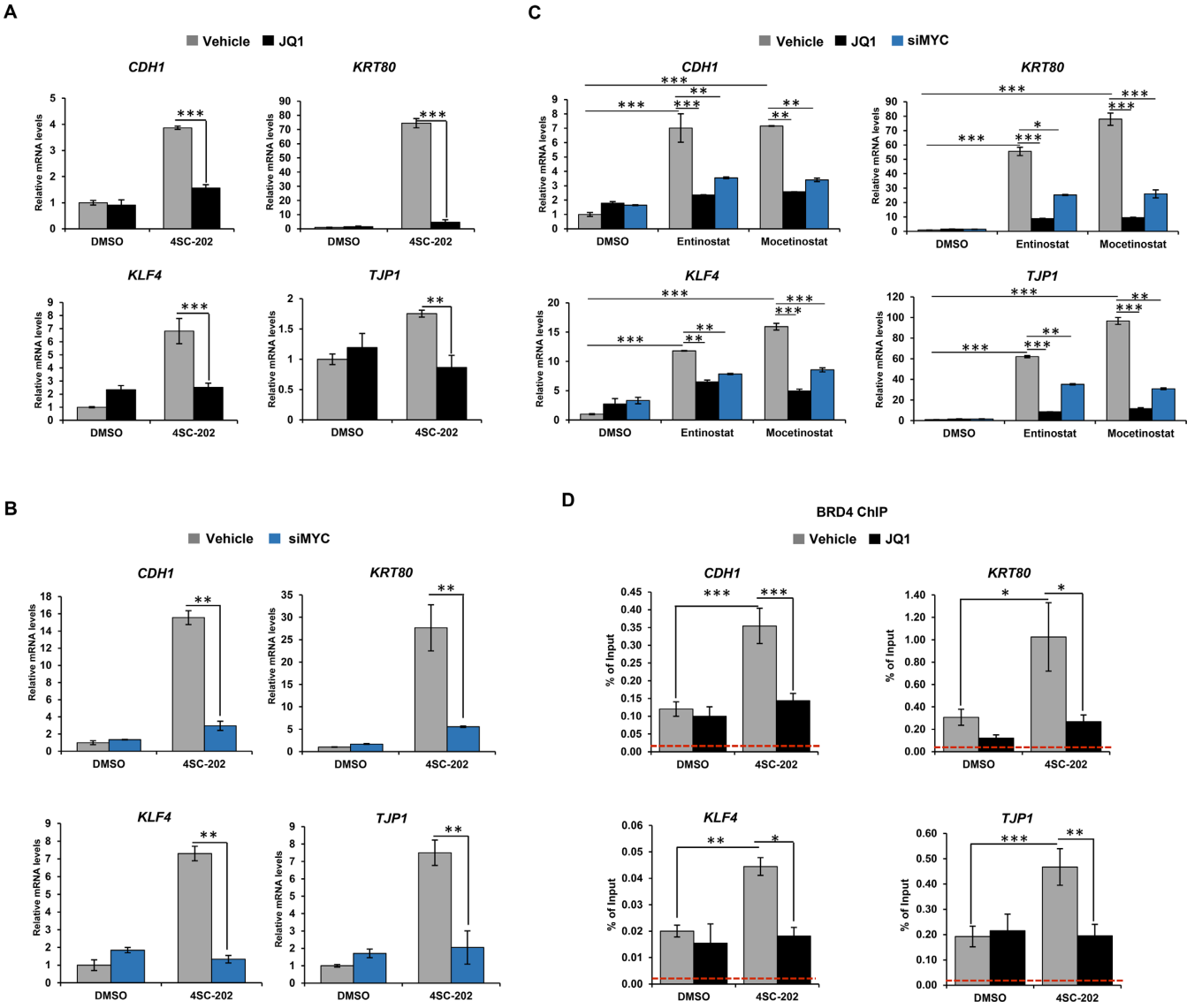

Figure 5. Genes induced by 4SC-202 treatment require BRD4 and MYC for their induction. (**A**, **B**) Gene expression analysis of *CDH1, KRT80, TJP1* and *KLF4* genes in L3.6 cells treated with JQ1 (250 nM) or depleted for MYC (siMYC) under control conditions or in combination with 4SC-202 (1 μM) treatment. Relative expression was analyzed by qRT-PCR and shown as 'relative mRNA levels' compared to the expression of an unregulated reference gene (*RPLP0*). Data are represented as mean ± SD. $n = 3$. ***$P \leq 0.005$, **$P \leq 0.01$, *$P \leq 0.05$. (**C**) Gene expression analysis of *CDH1*, *KRT80*, *TJP1* and *KLF4* genes in L3.6 cells treated with mocetinostat or entinostat (500 nM) with or without treatment with JQ1 (250 nM) or depletion of MYC (siMYC). (**D**) ChIP analysis of BRD4 on the *CDH1*, *KRT80*, *TJP1* and *KLF4* genes in L3.6 cells treated with vehicle, JQ1 (250 nM) or 4SC-202 (1 μM) as indicated. Immunoprecipitated DNA was compared to input and shown as percentage. IgG antibody was used as a negative control to indicate experimental background and is shown as a red dotted line. Data are represented as mean ± SD. $n = 3$.

lated genes displayed an overlap with regions occupied by both BRD4 and MYC from published datasets. To investigate the role of BRD4 and MYC in mediating gene induction following 4SC-202 treatment we examined a subset of genes (*CDH1, KRT80, TJP1 and KLF4)* associated with a more differentiated phenotype (53–59), which were upregulated in response to 4SC-202 treatment. Consistent with our genome-wide analyses, single gene ChIP-qPCR analyses confirmed that all four genes exhibited a notable increase in H3K27ac occupancy near the TSS following 4SC-202 treatment (Figure 4E and F). Taken together these results reveal that, while treatment with the HDACi 4SC-202 results in an increase in H3K27ac and H3K4me3 around the TSS of genes globally, genes upregulated in response to 4SC-202 display a co-occupancy of BRD4 and MYC.

BRD4 and MYC are required for 4SC-202-mediated upregulation of gene expression

Based on the enrichment of MYC and BRD4 on genes induced by 4SC-202 treatment as identified by ReMap analyses, we hypothesized that inhibition of BRD4 or siRNA-mediated depletion of MYC (siMYC) should block the HDACi-mediated induction of this subset of upregulated genes. Therefore, we utilized the small molecule inhibitor of the Bromodomain and Extraterminal (BET) family of

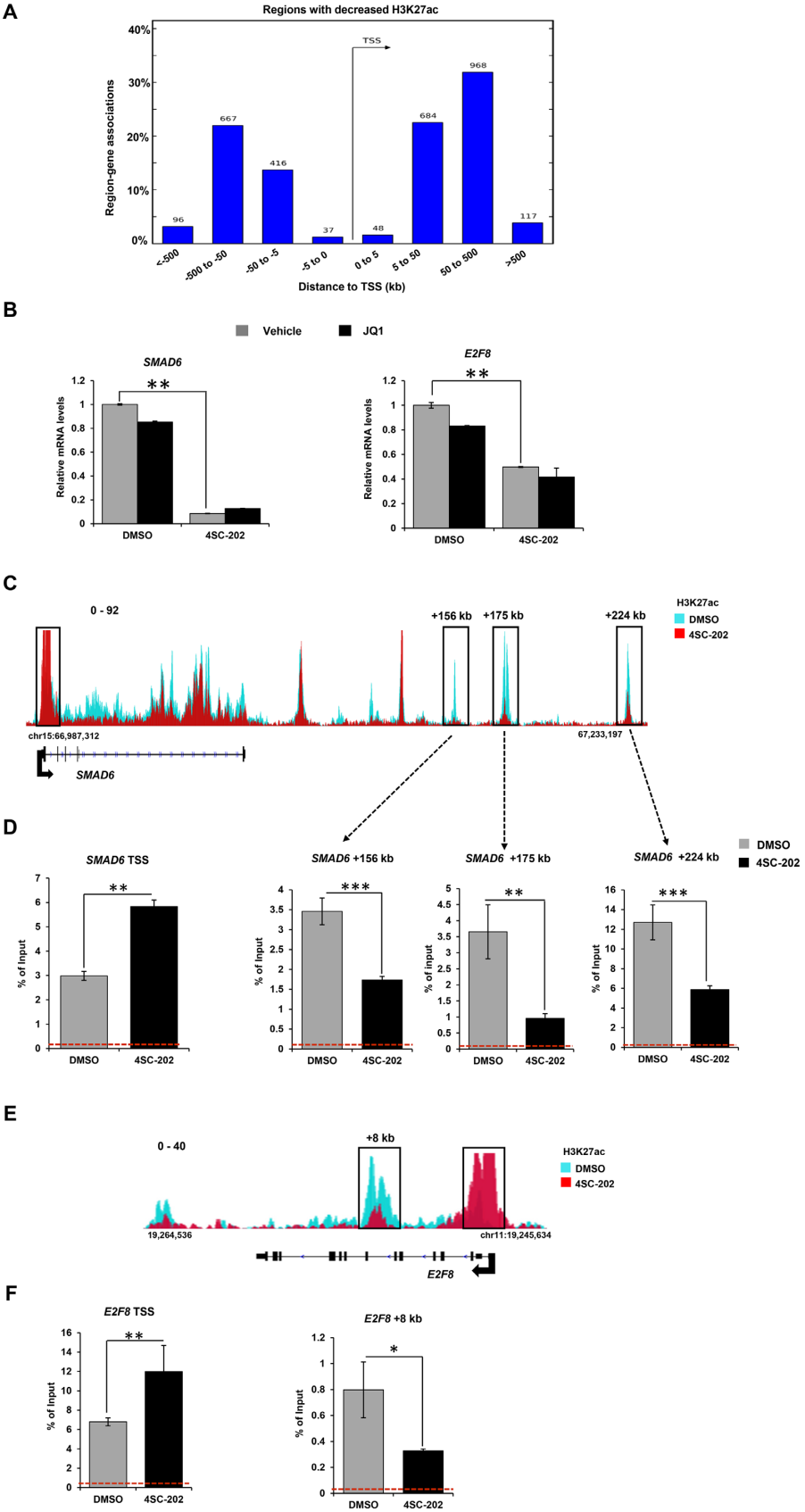

Figure 6. 4SC-202-mediated enhancer deactivation accompanies downregulation of a subset of genes. (**A**) GREAT analysis was performed on regions associated with decreased H3K27ac in response to 4SC-202 treatment obtained from DiffBind analysis. Bar graph from GREAT analysis shows the

factors (BETi), JQ1, which specifically prevents the binding of BRD4 to acetylated chromatin (20). Interestingly, treatment with JQ1 or siRNA-mediated depletion of MYC had no significant effects on the basal expression of the *CDH1, KRT80, TJP1* and *KLF4* genes, while significantly blocking the increase in gene expression in response to 4SC-202 treatment (Figure 5A and B). Consistent with this effect being a general consequence of class-I HDAC inhibition, mocetinostat and entinostat also elicited a significant increase in the expression of these genes, which could be efficiently blocked by JQ1 or siMYC treatment (Figure 5C). As a control, we also investigated the effects of BRD4 and MYC perturbation on the expression of *CDKN1A* and *CD24*. Interestingly, JQ1 treatment and MYC depletion each resulted in increased *CDKN1A* expression, even in the absence of 4SC-202 treatment, and had no or only modest effects on 4SC-202-induced expression. Similarly, JQ1 had no effect on either basal or 4SC-202-induced *CD24* expression, while MYC perturbation resulted in a slight increase in basal and reduction in 4SC-202-induced *CD24* expression (Supplementary Figure S3A and B).

We next performed ChIP-qPCR to examine BRD4 enrichment near the TSS of the *CDH1, KRT80, TJP1* and *KLF4* genes, to confirm its increased recruitment to upregulated genes upon 4SC-202 treatment as well as the ability of JQ1 to prevent this effect. Consistent with our gene expression studies, ChIP-qPCR results showed a significant increase in BRD4 recruitment in response to 4SC-202 treatment and this effect could be blocked by JQ1 treatment (Figure 5D). Together, these results reveal a positive and specific role of BRD4 and MYC in 4SC-202-induced increases in gene expression.

4SC-202-mediated enhancer deactivation is associated with gene repression

While the mechanisms by which HDACi active gene expression is relatively well understood, much less is known about how HDACi treatment leads to gene repression. Thus, we investigated the mechanism behind decreased expression of a subset of genes in response to 4SC-202 treatment. We performed GREAT analysis on the genomic regions which were associated with decreased H3K27ac upon 4SC-202 treatment. Interestingly, this revealed that decreased H3K27ac was associated primarily with regions distal to the TSS (±5–500 kb, Figure 6A). Moreover, regions with decreased H3K27ac were found to be associated with a subset of genes (e.g. *SMAD6* and *E2F8*) downregulated in response to 4SC-202 treatment. To confirm these findings, we performed gene expression analysis for *SMAD6* and *E2F8* and observed a significant reduction in their mRNA levels upon 4SC-202, but not JQ1 treatment (Figure 6B). Interestingly, both *SMAD6* and *E2F8* showed a marked increase in H3K27ac occupancy near the TSS, but significantly decreased occupancy at distal regions up- and downstream of the TSS (marked with black boxes; Figure 6C and E). This effect was verified by independent ChIP-qPCR studies, which confirmed a significant increase in H3K27ac occupancy at the TSS region of *SMAD6* and *E2F8*, but a marked decrease at the investigated distal sites (Figure 6D and F). Together these results revealed that the HDACi-mediated decrease in H3K27ac occupancy at the distal regions of a subset of genes is most likely associated with enhancer deactivation and an associated downregulation of target gene expression.

DISCUSSION

HDAC inhibitors have been the subject of significant interest and intense research due to their potential utility as anticancer therapeutic agents. However, in light of the very moderate clinical success as single agents in PDAC to date (9), a better understanding of their underlying molecular mechanisms of action will be essential for their optimal clinical utilization and combination with other agents. Here, we have examined the potential utility of the HDAC class-I-specific inhibitors 4SC-202, entinostat and mocetinostat to induce a more differentiated phenotype, as well as attenuating tumorigenic properties and cell proliferation in PDAC tumor cells.

Our results reveal that 4SC-202 attenuates TGFβ-induced EMT and restores the expression of a TGFβ-repressed gene signature in heterologous cell lines. Whole-exome sequencing studies have shown that the TGFβ pathway is frequently altered in PDAC (6), including the BxPC3 cell line used here (60). TGFβ is one of the most potent inducers of EMT and chemoresistant PDAC cells have been shown to display an EMT-like phenotype with enhanced migration and invasive capacity (61,62). TGFβ signaling has also been demonstrated to be associated with the production of extra-cellular matrix (ECM) proteins, major components of the stromal microenvironment in PDAC (63,64). Interestingly, 4SC-202-regulated genes were significantly enriched for extracellular matrix-associated gene sets. A recent study highlighted the potential role of HDAC class-I specific inhibitors in restoring chemosensitivity in resistant PDAC cells by inhibiting expression of the EMT-associated transcription factor ZEB1 (65). Moreover, ZEB1 and HDACs (HDAC1 and 2) were reported to be involved in the repression of E-cadherin *(CDH1)* expression in

←

association of decreased H3K27ac with distal regions (±5 kb from TSS). (**B**) Gene expression analysis of *SMAD6* and *E2F8* genes in L3.6 cells treated with 4SC-202 (1 μM) or JQ1 (250 nM) alone or in combination. Relative expression was analyzed by qRT-PCR and shown as 'relative mRNA levels' compared to the expression of an unregulated reference gene (*RPLP0*). Data are represented as mean ± SD. $n = 3$. ***$P \leq 0.005$, **$P \leq 0.01$, *$P \leq 0.05$. (**C**) H3K27ac profile for *SMAD6* in control (DMSO, blue) and 4SC-202-treated (red) conditions. The black arrow indicates the TSS and direction of transcription. (**D**) ChIP analysis of H3K27ac at TSS, +156, +175 and +224 kb regions of *SMAD6* in L3.6 cells treated with 4SC-202 (1 μM). Immunoprecipitated DNA was compared to input and shown as percentage. IgG antibody was used as a negative control to indicate experimental background levels and is shown as a red dotted line. Data are represented as mean ± SD. $n = 3$. (**E**) H3K27ac profile for *E2F8* in control (DMSO, black) and 4SC-202-treated (red) conditions. The black arrow indicates the TSS and direction of transcription. (**F**) ChIP analysis of H3K27ac at TSS and +8 kb regions of *E2F8* in L3.6 cells treated with 4SC-202. Immunoprecipitated DNA was compared to input and shown as percentage. IgG antibody was used as a negative control to determine experimental background and is shown as a red dotted line. Data are represented as mean ± SD. $n = 3$.

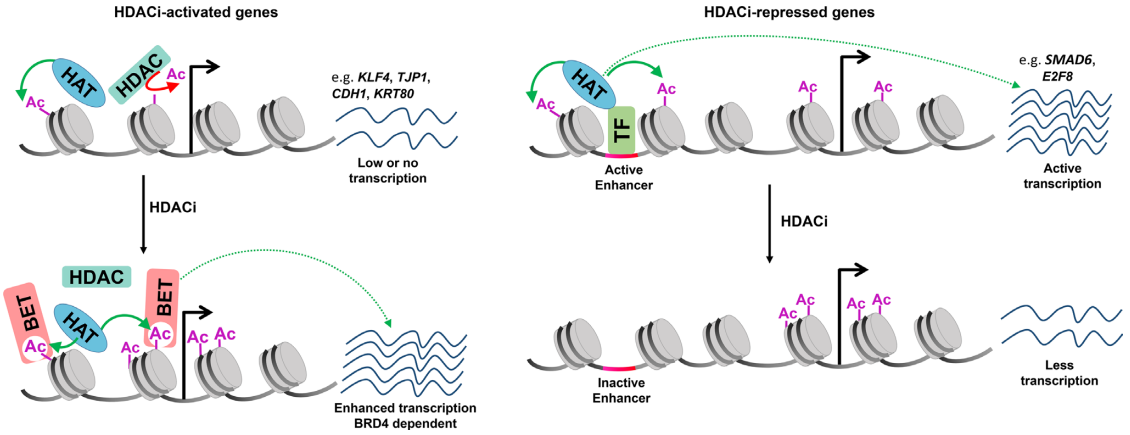

Figure 7. HDACi-mediated gene activation and repression rely upon distinct mechanisms. Proposed model illustrating distinct mechanisms of action of HDACi leading to gene activation and repression. HDACi-mediated gene activation (left) involves increased recruitment of BRD4 to TSS-proximal regions, resulting in enhanced transcription and subsequently increased expression. In contrast, HDACi-mediated gene repression results from decreased deacetylation at distal enhancer regions, leading to their deactivation and decreased transcription, despite increases in TSS-proximal acetylation.

PDAC, which was attenuated by HDACi treatment (66). Given the inhibitory function of 4SC-202 on EMT phenotype, our data suggest that the enhancement or restoration of chemosensitivity in PDAC cells may be a general feature of HDAC class-I inhibitors.

Inhibition of HDACs results in hyperacetylation of histones and other proteins which can impact transcription in both positive and negative ways. Interestingly, although both H3K27ac and H3K4me3 levels increased globally on all the genes analyzed, different subsets of genes displayed disparate responses to 4SC-202 treatment. Unexpectedly, the set of 4SC-202-induced genes displayed a significant enrichment of MYC and BRD4 occupancy. BRD4 is an acetyllysine reader and acts as a transcriptional activator by promoting the activity of the Positive Transcription Elongation Factor-b (P-TEFb) and transcriptional elongation (67–69). Markedly, perturbations in BRD4 or MYC function significantly inhibited the ability of 4SC-202 to induce the expression of genes associated with a differentiated (*KRT80*, *KLF4*) and epithelial (*CDH1*, *TJP1*) cell phenotype. Moreover, these effects were specific since *CDKN1A* (encoding p21) and *CD24*, which were not identified as direct BRD4 and MYC targets, were not as dramatically affected by BRD4 or MYC perturbation. Based on these findings we hypothesize that HDACi-mediated induction of gene expression occurs in cooperation with BRD4 and MYC.

MYC is one the most studied human oncogenes and has been frequently associated with tumor growth and progression due to its involvement in a myriad of biological processes including cell growth, proliferation and apoptosis. Interestingly, apart from its oncogenic function in promoting tumor cell proliferation, MYC also stimulates epidermal differentiation in a concentration-dependent manner (70,71). Similarly, another study uncovered a potential mechanism by which MYC promoted epithelial differentiation of prostate cancer cells by promoting the transient expression of ING4 (72). It is conceivable that HDACi treatment may somehow attenuate oncogenic MYC function and restore a more physiological differentiation-promoting function of MYC. Additional studies will be necessary to further uncover the importance of MYC and underlying mechanisms in HDACi-induced differentiation of PDAC cells.

Our data revealed that HDACi treatment led to decreased H3K27ac occupancy at some regions distal to the TSS. Recently it was reported that HDAC inhibition leads to reduced BRD4 occupancy at enhancer regions (73). Interestingly, while our data reveal that HDACi treatment results in decreased H3K27ac occupancy at a subset of distal sites, we could not detect BRD4 at these sites (data not shown). Consistently, the expression of these genes was insensitive to JQ1 treatment, suggesting that different subsets of enhancers are differentially affected by HDACi and BETi. According to these findings we propose a model (Figure 7) in which genes induced by HDACi treatment rely primarily on increased BRD4 recruitment to the TSS-proximal region, likely mediated via increased acetylation. In contrast, genes which are down-regulated following HDACi treatment rely upon BRD4-independent distal enhancer regions, which display decreased H3K27ac levels. We hypothesize that these effects may be mediated by decreased recruitment or activity of specific transcription factors, whose function may require deacetylation.

Interestingly, while our data show that BRD4 is, in fact, required for the induction of a subset of differentiation-related genes in response to HDACi in PDAC cells, the relationship between HDACi and BETi treatment is complex. Importantly, while BETi show significant effects in monotherapy (74,75), a recent study demonstrated a synergistic anti-tumor effect of BETi and HDACi combination therapy in an established PDAC genetically engineered mouse model (31). It is conceivable, that the simultaneous targeting of both BRD4-dependent (i.e. BETi-sensitive) and BRD4-independent (i.e. HDACi-sensitive) enhancers may provide synergistic effects on the overall transcriptional profile of PDAC cells, thereby increasing the potency of either treatment alone. Furthermore, the heterogeneity of pancreatic tumors *in vivo*, in which the cellularity of PDAC is low and tumors display a high stromal content, results in

a significantly higher complexity involving interactions and activity of tumor cells, cancer-associated fibroblasts and immune cells, which cannot adequately be recapitulated *in vitro*. Thus, in order to gain additional insight into the relationship between HDACi and BETi in PDAC additional transcriptome- and genome-wide studies *in vitro*, accompanied by corresponding *in vivo* studies, will be necessary to uncover both molecular mechanisms of action as well as the suitability of combination therapy for clinical application.

In conclusion, we have identified an unexpected functional importance of BRD4 and MYC in eliciting the HDACi-mediated effects on the induction of gene expression, thereby revealing a previously unknown mechanism by which perceived oncogenic transcriptional regulatory mechanisms may potentially be exploited for anti-tumor therapy.

ACCESSION NUMBERS

ChIP-Seq and RNA-Seq data have been deposited in Gene Expression Omnibus and are available under the accession number GSE90112.

SUPPLEMENTARY DATA

Supplementary Data are available at NAR Online.

ACKNOWLEDGEMENTS

The authors thank G. Salinas and F. Ludewig for performing next generation sequencing, S. Knapp for providing JQ1, P. Altevogt for providing the CD24 antibody, F. Hamdan, X. Wang, O. Hahn, L. Chua and the rest of the Johnsen group for helpful discussions.

Author contributions: The experiments were designed by S.A.J. and V.K.M. with input from F.W., R.L.K., Z.N., R.B., J.T.S., T.W., H.K. and E.H. V.K.M. performed cell culture experiments, generated all high throughput sequencing data and performed bioinformatic analyses. M.S. provided assistance in gene expression studies. Z.N. provided support with bioinformatic analyses. V.K.M., R.L.K. and F.W. performed xenograft studies and analysis of tumor growth *in vivo*. Immunohistochemical analyses were verified by H.U.S. The manuscript was written by V.K.M. and S.A.J. All authors read and approved the manuscript.

FUNDING

4SC AG and by the Deutsche Krebshilfe consortium for Translational Oncology entitled 'Targeting Plasticity in Pancreatic Ductal AdenoCarcinoma' [70112505 to J.T.S., E.H., S.A.J.] (in part) Funding for open access charge: Internal institutional.

Conflict of interest statement. Roland Baumgartner, Hella Kohlhof and Tanja Wulff are employed by 4SC AG, which owns the investigated substance 4SC-202.

REFERENCES

1. Adiseshaiah,P.P., Crist,R.M., Hook,S.S. and McNeil,S.E. (2016) Nanomedicine strategies to overcome the pathophysiological barriers of pancreatic cancer. *Nat. Rev. Clin. Oncol.*, **13**, 750–765.
2. Jones,S., Zhang,X., Parsons,D.W., Lin,J.C.-H., Leary,R.J., Angenendt,P., Mankoo,P., Carter,H., Kamiyama,H., Jimeno,A. *et al.* (2008) Core signaling pathways in human pancreatic cancers revealed by global genomic analyses. *Science*, **321**, 1801–1806.
3. Hidalgo,M. (2010) Pancreatic cancer. *N. Engl. J. Med.*, **362**, 1605–1617.
4. Bailey,P., Chang,D.K., Nones,K., Johns,A.L., Patch,A.-M., Gingras,M.-C., Miller,D.K., Christ,A.N., Bruxner,T.J.C., Quinn,M.C. *et al.* (2016) Genomic analyses identify molecular subtypes of pancreatic cancer. *Nature*, **531**, 47–52.
5. Shain,A.H., Salari,K., Giacomini,C.P. and Pollack,J.R. (2013) Integrative genomic and functional profiling of the pancreatic cancer genome. *BMC Genomics*, **14**, 624.
6. Waddell,N., Pajic,M., Patch,A.-M., Chang,D.K., Kassahn,K.S., Bailey,P., Johns,A.L., Miller,D., Nones,K., Quek,K. *et al.* (2015) Whole genomes redefine the mutational landscape of pancreatic cancer. *Nature*, **518**, 495–501.
7. Biankin,A.V., Waddell,N., Kassahn,K.S., Gingras,M.-C., Muthuswamy,L.B., Johns,A.L., Miller,D.K., Wilson,P.J., Patch,A.-M., Wu,J. *et al.* (2012) Pancreatic cancer genomes reveal aberrations in axon guidance pathway genes. *Nature*, **491**, 399–405.
8. Witkiewicz,A.K., McMillan,E.A., Balaji,U., Baek,G., Lin,W.-C., Mansour,J., Mollaee,M., Wagner,K.-U., Koduru,P., Yopp,A. *et al.* (2015) Whole-exome sequencing of pancreatic cancer defines genetic diversity and therapeutic targets. *Nat. Commun.*, **6**, 6744.
9. Hessmann,E., Johnsen,S.A., Siveke,J.T. and Ellenrieder,V. (2016) Epigenetic treatment of pancreatic cancer: is there a therapeutic perspective on the horizon? *Gut*, doi:10.1136/gutjnl-2016-312539.
10. Glozak,M.A. and Seto,E. (2007) Histone deacetylases and cancer. *Oncogene*, **26**, 5420–5432.
11. Bolden,J.E., Peart,M.J. and Johnstone,R.W. (2006) Anticancer activities of histone deacetylase inhibitors. *Nat. Rev. Drug Discov.*, **5**, 769–784.
12. Damaskos,C., Karatzas,T., Nikolidakis,L., Kostakis,I.D., Karamaroudis,S., Boutsikos,G., Damaskou,Z., Kostakis,A. and Kouraklis,G. (2015) Histone deacetylase (HDAC) inhibitors: current evidence for therapeutic activities in pancreatic cancer. *Anticancer Res.*, **35**, 3129–3135.
13. Koutsounas,I., Giaginis,C. and Theocharis,S. (2013) Histone deacetylase inhibitors and pancreatic cancer: are there any promising clinical trials? *World J. Gastroenterol. WJG*, **19**, 1173–1181.
14. Fritsche,P., Seidler,B., Schüler,S., Schnieke,A., Göttlicher,M., Schmid,R.M., Saur,D. and Schneider,G. (2009) HDAC2 mediates therapeutic resistance of pancreatic cancer cells via the BH3-only protein NOXA. *Gut*, **58**, 1399–1409.
15. Schneider,G., Krämer,O.H., Fritsche,P., Schüler,S., Schmid,R.M. and Saur,D. (2010) Targeting histone deacetylases in pancreatic ductal adenocarcinoma. *J. Cell. Mol. Med.*, **14**, 1255–1263.
16. Marks,P.A., Rifkind,R.A., Richon,V.M., Breslow,R., Miller,T. and Kelly,W.K. (2001) Histone deacetylases and cancer: causes and therapies. *Nat. Rev. Cancer*, **1**, 194–202.
17. Wang,G., He,J., Zhao,J., Yun,W., Xie,C., Taub,J.W., Azmi,A., Mohammad,R.M., Dong,Y., Kong,W. *et al.* (2012) Class I and class II histone deacetylases are potential therapeutic targets for treating pancreatic cancer. *PLoS ONE*, **7**, e52095.
18. Schüler,S., Fritsche,P., Diersch,S., Arlt,A., Schmid,R.M., Saur,D. and Schneider,G. (2010) HDAC2 attenuates TRAIL-induced apoptosis of pancreatic cancer cells. *Mol. Cancer*, **9**, 80.
19. Filippakopoulos,P., Picaud,S., Mangos,M., Keates,T., Lambert,J.-P., Barsyte-Lovejoy,D., Felletar,I., Volkmer,R., Müller,S., Pawson,T. *et al.* (2012) Histone recognition and large-scale structural analysis of the human bromodomain family. *Cell*, **149**, 214–231.
20. Filippakopoulos,P., Qi,J., Picaud,S., Shen,Y., Smith,W.B., Fedorov,O., Morse,E.M., Keates,T., Hickman,T.T., Felletar,I. *et al.* (2010) Selective inhibition of BET bromodomains. *Nature*, **468**, 1067–1073.
21. Nicodeme,E., Jeffrey,K.L., Schaefer,U., Beinke,S., Dewell,S., Chung,C., Chandwani,R., Marazzi,I., Wilson,P., Coste,H. *et al.* (2010) Suppression of inflammation by a synthetic histone mimic. *Nature*, **468**, 1119–1123.
22. Zuber,J., Shi,J., Wang,E., Rappaport,A.R., Herrmann,H., Sison,E.A., Magoon,D., Qi,J., Blatt,K., Wunderlich,M. *et al.* (2011) RNAi screen identifies Brd4 as a therapeutic target in acute myeloid leukaemia. *Nature*, **478**, 524–528.

23. Dawson,M.A., Prinjha,R.K., Dittmann,A., Giotopoulos,G., Bantscheff,M., Chan,W.-I., Robson,S.C., Chung,C., Hopf,C., Savitski,M.M. *et al.* (2011) Inhibition of BET recruitment to chromatin as an effective treatment for MLL-fusion leukaemia. *Nature*, **478**, 529–533.
24. Delmore,J.E., Issa,G.C., Lemieux,M.E., Rahl,P.B., Shi,J., Jacobs,H.M., Kastritis,E., Gilpatrick,T., Paranal,R.M., Qi,J. *et al.* (2011) BET bromodomain inhibition as a therapeutic strategy to target c-Myc. *Cell*, **146**, 904–917.
25. Puissant,A., Frumm,S.M., Alexe,G., Bassil,C.F., Qi,J., Chanthery,Y.H., Nekritz,E.A., Zeid,R., Gustafson,W.C., Greninger,P. *et al.* (2013) Targeting MYCN in neuroblastoma by BET bromodomain inhibition. *Cancer Discov.*, **3**, 308–323.
26. Asangani,I.A., Dommeti,V.L., Wang,X., Malik,R., Cieslik,M., Yang,R., Escara-Wilke,J., Wilder-Romans,K., Dhanireddy,S., Engelke,C. *et al.* (2014) Therapeutic targeting of BET bromodomain proteins in castration-resistant prostate cancer. *Nature*, **510**, 278–282.
27. Coudé,M.-M., Braun,T., Berrou,J., Dupont,M., Bertrand,S., Masse,A., Raffoux,E., Itzykson,R., Delord,M., Riveiro,M.E. *et al.* (2015) BET inhibitor OTX015 targets BRD2 and BRD4 and decreases c-MYC in acute leukemia cells. *Oncotarget*, **6**, 17698–17712.
28. Nagarajan,S., Hossan,T., Alawi,M., Najafova,Z., Indenbirken,D., Bedi,U., Taipaleenmäki,H., Ben-Batalla,I., Scheller,M., Loges,S. *et al.* (2014) Bromodomain protein BRD4 is required for estrogen receptor-dependent enhancer activation and gene transcription. *Cell Rep.*, **8**, 460–469.
29. Nagarajan,S., Bedi,U., Budida,A., Hamdan,F.H., Mishra,V.K., Najafova,Z., Xie,W., Alawi,M., Indenbirken,D., Knapp,S. *et al.* BRD4 promotes p63 and GRHL3 expression downstream of FOXO in mammary epithelial cells. *Nucleic Acids Res.*, doi:10.1093/nar/gkw1276.
30. Najafova,Z., Tirado-Magallanes,R., Subramaniam,M., Hossan,T., Schmidt,G., Nagarajan,S., Baumgart,S.J., Mishra,V.K., Bedi,U., Hesse,E. *et al.* (2016) BRD4 localization to lineage-specific enhancers is associated with a distinct transcription factor repertoire. *Nucleic Acids Res.*, doi:10.1093/nar/gkw826.
31. Mazur,P.K., Herner,A., Mello,S.S., Wirth,M., Hausmann,S., Sánchez-Rivera,F.J., Lofgren,S.M., Kuschma,T., Hahn,S.A., Vangala,D. *et al.* (2015) Combined inhibition of BET family proteins and histone deacetylases as a potential epigenetics-based therapy for pancreatic ductal adenocarcinoma. *Nat. Med.*, **21**, 1163–1171.
32. Prenzel,T., Begus-Nahrmann,Y., Kramer,F., Hennion,M., Hsu,C., Gorsler,T., Hintermair,C., Eick,D., Kremmer,E., Simons,M. *et al.* (2011) Estrogen-dependent gene transcription in human breast cancer cells relies upon proteasome-dependent monoubiquitination of histone H2B. *Cancer Res.*, **71**, 5739–5753.
33. Mishra,V.K., Subramaniam,M., Kari,V., Pitel,K.S., Baumgart,S.J., Naylor,R.M., Nagarajan,S., Wegwitz,F., Ellenrieder,V., Hawse,J.R. *et al.* (2017) Krüppel-like transcription factor KLF10 suppresses TGFβ-induced epithelial-to-mesenchymal transition via a negative feedback mechanism. *Cancer Res.*, doi:10.1158/0008-5472.CAN-16-2589.
34. Schneider,C.A., Rasband,W.S. and Eliceiri,K.W. (2012) NIH image to ImageJ: 25 years of image analysis. *Nat. Methods*, **9**, 671–675.
35. Singh,S.K., Chen,N.-M., Hessmann,E., Siveke,J., Lahmann,M., Singh,G., Voelker,N., Vogt,S., Esposito,I., Schmidt,A. *et al.* (2015) Antithetical NFATc1–Sox2 and p53–miR200 signaling networks govern pancreatic cancer cell plasticity. *EMBO J.*, **34**, 517–530.
36. Babraham bioinformatics - FastQC a quality control tool for high throughput sequence data.
37. Langmead,B. and Salzberg,S.L. (2012) Fast gapped-read alignment with Bowtie 2. *Nat. Methods*, **9**, 357–359.
38. Zhang,Y., Liu,T., Meyer,C.A., Eeckhoute,J., Johnson,D.S., Bernstein,B.E., Nusbaum,C., Myers,R.M., Brown,M., Li,W. *et al.* (2008) Model-based analysis of ChIP-Seq (MACS). *Genome Biol.*, **9**, R137.
39. Ramírez,F., Dündar,F., Diehl,S., Grüning,B.A. and Manke,T. (2014) deepTools: a flexible platform for exploring deep-sequencing data. *Nucleic Acids Res.*, **42**, W187–W191.
40. Robinson,J.T., Thorvaldsdóttir,H., Winckler,W., Guttman,M., Lander,E.S., Getz,G. and Mesirov,J.P. (2011) Integrative genomics viewer. *Nat. Biotechnol.*, **29**, 24–26.
41. Ross-Innes,C.S., Stark,R., Teschendorff,A.E., Holmes,K.A., Ali,H.R., Dunning,M.J., Brown,G.D., Gojis,O., Ellis,I.O., Green,A.R. *et al.* (2012) Differential oestrogen receptor binding is associated with clinical outcome in breast cancer. *Nature*, **481**, 389–393.
42. McLean,C.Y., Bristor,D., Hiller,M., Clarke,S.L., Schaar,B.T., Lowe,C.B., Wenger,A.M. and Bejerano,G. (2010) GREAT improves functional interpretation of cis-regulatory regions. *Nat. Biotechnol.*, **28**, 495–501.
43. Griffon,A., Barbier,Q., Dalino,J., van Helden,J., Spicuglia,S. and Ballester,B. (2014) Integrative analysis of public ChIP-seq experiments reveals a complex multi-cell regulatory landscape. *Nucleic Acids Res.*, doi:10.1093/nar/gku1280.
44. Anders,S., Pyl,P.T. and Huber,W. (2015) HTSeq—a Python framework to work with high-throughput sequencing data. *Bioinformatics*, **31**, 166–169.
45. Love,M.I., Huber,W. and Anders,S. (2014) Moderated estimation of fold change and dispersion for RNA-seq data with DESeq2. *Genome Biol.*, **15**, 550.
46. Pinkerneil,M., Hoffmann,M.J., Kohlhof,H., Schulz,W.A. and Niegisch,G. (2016) Evaluation of the therapeutic potential of the novel isotype specific HDAC inhibitor 4SC-202 in urothelial carcinoma cell lines. *Target. Oncol.*, **11**, 783–798.
47. Richon,V.M., Sandhoff,T.W., Rifkind,R.A. and Marks,P.A. (2000) Histone deacetylase inhibitor selectively induces p21WAF1 expression and gene-associated histone acetylation. *Proc. Natl. Acad. Sci. U.S.A.*, **97**, 10014–10019.
48. Muscat,A., Popovski,D., Jayasekara,W.S.N., Rossello,F.J., Ferguson,M., Marini,K.D., Alamgeer,M., Algar,E.M., Downie,P., Watkins,D.N. *et al.* (2016) Low-dose histone deacetylase inhibitor treatment leads to tumor growth arrest and multi-lineage differentiation of malignant rhabdoid tumors. *Clin. Cancer Res.*, **22**, 3560–3570.
49. Munster,P.N., Troso-Sandoval,T., Rosen,N., Rifkind,R., Marks,P.A. and Richon,V.M. (2001) The histone deacetylase inhibitor suberoylanilide hydroxamic acid induces differentiation of human breast cancer cells. *Cancer Res.*, **61**, 8492–8497.
50. Lubeseder-Martellato,C., Hidalgo-Sastre,A., Hartmann,C., Alexandrow,K., Kamyabi-Moghaddam,Z., Sipos,B., Wirth,M., Neff,F., Reichert,M., Heid,I. *et al.* (2014) Membranous CD24 drives the epithelial phenotype of pancreatic cancer. *Oncotarget*, doi:10.18632/oncotarget.9402.
51. Visvader,J.E. and Lindeman,G.J. (2008) Cancer stem cells in solid tumours: accumulating evidence and unresolved questions. *Nat. Rev. Cancer*, **8**, 755–768.
52. Ellenrieder,V., Hendler,S.F., Boeck,W., Seufferlein,T., Menke,A., Ruhland,C., Adler,G. and Gress,T.M. (2001) Transforming growth factor β1 treatment leads to an epithelial-mesenchymal transdifferentiation of pancreatic cancer cells requiring extracellular signal-regulated kinase 2 activation. *Cancer Res.*, **61**, 4222–4228.
53. Hong,S.-M., Li,A., Olino,K., Wolfgang,C.L., Herman,J.M., Schulick,R.D., Iacobuzio-Donahue,C., Hruban,R.H. and Goggins,M. (2011) Loss of E-cadherin expression and outcome among patients with resectable pancreatic adenocarcinomas. *Mod. Pathol.*, **24**, 1237–1247.
54. Georgiadis,A., Tschernutter,M., Bainbridge,J.W.B., Balaggan,K.S., Mowat,F., West,E.L., Munro,P.M.G., Thrasher,A.J., Matter,K., Balda,M.S. *et al.* (2010) The tight junction associated signalling proteins ZO-1 and ZONAB regulate retinal pigment epithelium homeostasis in mice. *PLoS ONE*, **5**, e15730.
55. Ni,S., Xu,L., Huang,J., Feng,J., Zhu,H., Wang,G. and Wang,X. (2013) Increased ZO-1 expression predicts valuable prognosis in non-small cell lung cancer. *Int. J. Clin. Exp. Pathol.*, **6**, 2887–2895.
56. Orbán,E., Szabó,E., Lotz,G., Kupcsulik,P., Páska,C., Schaff,Z. and Kiss,A. (2008) Different expression of occludin and ZO-1 in primary and metastatic liver tumors. *Pathol. Oncol. Res.*, **14**, 299–306.
57. Katz,J.P., Perreault,N., Goldstein,B.G., Lee,C.S., Labosky,P.A., Yang,V.W. and Kaestner,K.H. (2002) The zinc-finger transcription factor Klf4 is required for terminal differentiation of goblet cells in the colon. *Development*, **129**, 2619–2628.
58. Morris,V.A., Cummings,C.L., Korb,B., Boaglio,S. and Oehler,V.G. (2016) Deregulated KLF4 expression in myeloid leukemias alters cell proliferation and differentiation through microRNA and gene targets. *Mol. Cell. Biol.*, **36**, 559–573.
59. Langbein,L., Eckhart,L., Rogers,M.A., Praetzel-Wunder,S. and Schweizer,J. (2010) Against the rules: human Keratin K80: two

functional alternative splice variants, K80 AND K80.1, with special cellular localization in a wide range of epithelia. *J. Biol. Chem.*, **285**, 36909–36921.
60. Hahn,S.A., Schutte,M., Hoque,A.T.M.S., Moskaluk,C.A., Costa,L.T. da, Rozenblum,E., Weinstein,C.L., Fischer,A., Yeo,C.J., Hruban,R.H. *et al.* (1996) DPC4, a candidate tumor suppressor gene at human chromosome 18q21.1. *Science*, **271**, 350–353.
61. Arumugam,T., Ramachandran,V., Fournier,K.F., Wang,H., Marquis,L., Abbruzzese,J.L., Gallick,G.E., Logsdon,C.D., McConkey,D.J. and Choi,W. (2009) Epithelial to mesenchymal transition contributes to drug resistance in pancreatic cancer. *Cancer Res.*, **69**, 5820–5828.
62. Shah,A.N., Summy,J.M., Zhang,J., Park,S.I., Parikh,N.U. and Gallick,G.E. (2007) Development and characterization of gemcitabine-resistant pancreatic tumor cells. *Ann. Surg. Oncol.*, **14**, 3629–3637.
63. Bachem,M.G., Schünemann,M., Ramadani,M., Siech,M., Beger,H., Buck,A., Zhou,S., Schmid-Kotsas,A. and Adler,G. (2005) Pancreatic carcinoma cells induce fibrosis by stimulating proliferation and matrix synthesis of stellate cells. *Gastroenterology*, **128**, 907–921.
64. Löhr,M., Schmidt,C., Ringel,J., Kluth,M., Müller,P., Nizze,H. and Jesnowski,R. (2001) Transforming growth factor-β1 induces desmoplasia in an experimental model of human pancreatic carcinoma. *Cancer Res.*, **61**, 550–555.
65. Meidhof,S., Brabletz,S., Lehmann,W., Preca,B.-T., Mock,K., Ruh,M., Schüler,J., Berthold,M., Weber,A., Burk,U. *et al.* (2015) ZEB1-associated drug resistance in cancer cells is reversed by the class I HDAC inhibitor mocetinostat. *EMBO Mol. Med.*, **7**, 831–847.
66. Aghdassi,A., Sendler,M., Guenther,A., Mayerle,J., Behn,C.-O., Heidecke,C.-D., Friess,H., Büchler,M., Evert,M., Lerch,M.M. *et al.* (2012) Recruitment of histone deacetylases HDAC1 and HDAC2 by the transcriptional repressor ZEB1 downregulates E-cadherin expression in pancreatic cancer. *Gut*, **61**, 439–448.
67. Kanno,T., Kanno,Y., LeRoy,G., Campos,E., Sun,H.-W., Brooks,S.R., Vahedi,G., Heightman,T.D., Garcia,B.A., Reinberg,D. *et al.* (2014) BRD4 assists elongation of both coding and enhancer RNAs by interacting with acetylated histones. *Nat. Struct. Mol. Biol.*, **21**, 1047–1057.
68. Kanno,T., Kanno,Y., Siegel,R.M., Jang,M.K., Lenardo,M.J. and Ozato,K. (2004) Selective recognition of acetylated histones by bromodomain proteins visualized in living cells. *Mol. Cell*, **13**, 33–43.
69. Jang,M.K., Mochizuki,K., Zhou,M., Jeong,H.-S., Brady,J.N. and Ozato,K. (2005) The bromodomain protein Brd4 Is a positive regulatory component of P-TEFb and stimulates RNA polymerase II-dependent transcription. *Mol. Cell*, **19**, 523–534.
70. Berta,M.A., Baker,C.M., Cottle,D.L. and Watt,F.M. (2009) Dose and context dependent effects of Myc on epidermal stem cell proliferation and differentiation. *EMBO Mol. Med.*, **2**, 16–25.
71. Watt,F.M., Frye,M. and Benitah,S.A. (2008) MYC in mammalian epidermis: how can an oncogene stimulate differentiation? *Nat. Rev. Cancer*, **8**, 234–242.
72. Berger,P.L., Frank,S.B., Schulz,V.V., Nollet,E.A., Edick,M.J., Holly,B., Chang,T.-T.A., Hostetter,G., Kim,S. and Miranti,C.K. (2014) Transient induction of ING4 by Myc drives prostate epithelial cell differentiation and its disruption drives prostate tumorigenesis. *Cancer Res.*, **74**, 3357–3368.
73. Greer,C.B., Tanaka,Y., Kim,Y.J., Xie,P., Zhang,M.Q., Park,I.-H. and Kim,T.H. (2015) Histone deacetylases positively regulate transcription through the elongation machinery. *Cell Rep.*, **13**, 1444–1455.
74. Bian,B., Bigonnet,M., Gayet,O., Loncle,C., Maignan,A., Gilabert,M., Moutardier,V., Garcia,S., Turrini,O., Delpero,J.-R. *et al.* (2017) Gene expression profiling of patient-derived pancreatic cancer xenografts predicts sensitivity to the BET bromodomain inhibitor JQ1: implications for individualized medicine efforts. *EMBO Mol. Med.*, doi:10.15252/emmm.201606975.
75. Garcia,P.L., Miller,A.L., Kreitzburg,K.M., Council,L.N., Gamblin,T.L., Christein,J.D., Heslin,M.J., Arnoletti,J.P., Richardson,J.H., Chen,D. *et al.* (2016) The BET bromodomain inhibitor JQ1 suppresses growth of pancreatic ductal adenocarcinoma in patient-derived xenograft models. *Oncogene*, **35**, 833–845.